

## **FINITE ELEMENT SIMULATION OF THE EXCAVATION-INDUCED DEFORMATION IN TUNNELS DRIVEN IN POROELASTIC MEDIA**

**Evandro Pandia Cayro**

**Samir Maghous**

**Denise Bernaud Maghous**

*evandro.pandia@ufrgs.br*

*samir.maghous@ufrgs.br*

*denise.bernaud@ufrgs.br*

*Federal University of Rio Grande do Sul, Department of Civil Engineering Av. Osvaldo Aranha 99, 3rd floor, Centro – CEP 90035-190 – Porto Alegre, RS, Brazil*

**Abstract.** The present paper deals with the formulation of a constitutive and computational model for the analysis of the deformations induced by the excavation of a tunnel in a saturated poroelastic medium. The finite element implementation relies upon the discretization of weak forms of local momentum and fluid mass balance equations in the context of infinitesimal skeleton strains. The simulations of the steps of excavation as well as placement of the concrete lining are modeled by the method of activating/deactivating elements. The accuracy of the finite element approach is assessed by comparison with available analytical and semi-analytical solutions developed for a circular tunnel driven in a poroelastic medium. The numerical simulations notably show that the strain and stress fields developed around the tunnel will depend on the depth, cross-section geometry, surface load distribution, soil poroelastic properties, permeability coefficient and soil porosity. They also allow for the calculation of seepage forces due to pressure gradient induced by excavation and acting on the tunnel wall and tunnel face.

**Keywords:** Poroelastic medium, tunnel, excavation process, finite element simulation

## Introduction

The majority of tunnels are built in rockmass with presence of water, they are composed of rocks with fractured surfaces, through which the fluid moves causing problems of infiltration, it means ground with a high permeability. Infiltration of the fluid in the tunnel is also an important problem that must be considered in the design, construction and operation of the tunnel. Waterproofing and leak control saw the key in the construction of tunnels.

The sequence of the excavation advances is illustrated in Carranza-Torres and Fairhurst [1] (Fig. 1). The sequence starts at time  $t_0$  (Fig.1a) in which the liner has been installed at section A-A, located at a distance  $L_0$  from the face and the ground has converged radially by the amount of  $u_r^0$ . At this initial time  $t_0$ , the liner carries no load, i.e.,  $p_s = p_s^0$ . As the tunnel advances (Fig.1b), the support at section A-A is now located at the distance  $L_t$  from the face and carries the partial load  $p_s^t$  that the face had been carrying previously. At the instant  $t$ , the ground deforms by amount  $u_r^t$ . Once the tunnel has advanced far enough from section A-A (Fig.1c), spanning a distance  $L_F$  from the face, the face effect disappears. The support will carry the full excavation load  $p_s^F$  and the tunnel will converge to its maximum radial displacement  $u_r^{max}$ .

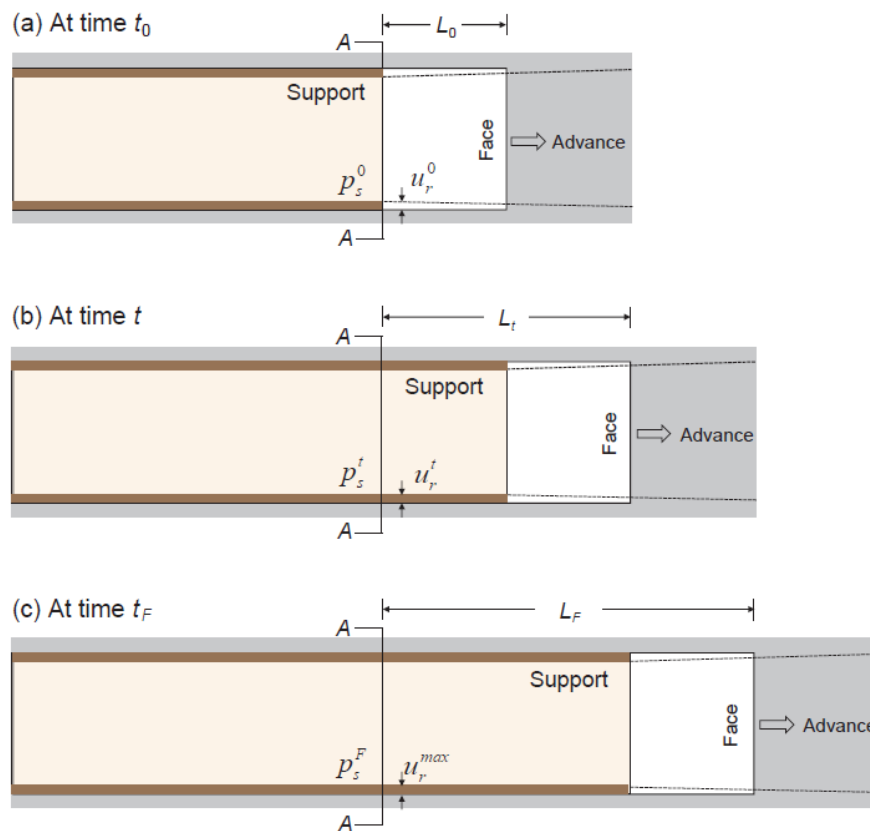


Figure 1. Illustration of support pressure  $p_s$  and radial displacement  $u_r$  at section A-A due to tunnel advance as adapted from Carranza-Torres and Fairhurst [1]

In tunnel with saturated ground, it exists a transient process, two important states can be distinguished: the state immediately after excavation (i.e., at time  $t = 0^+$ ) and the long term one ( $t = \infty$ ). The first state is characterized by the condition of constant water content (“undrained conditions”), the second state is governed by the steady state pore pressure distribution (“drained conditions”). In the

drained conditions the pore pressure buildup obtained in undrained conditions will dissipate as the ground is consolidating.

## 1 Poroelastic model and excavation procedure

### 1.1 Field Equations

The present work adopt the hypothesis of small perturbations that includes the following hypothesis: infinitesimal transformations, small displacements for the skeleton particles, small variations of Lagrangian porosity, small variations of the fluid mass density. Therefore the general expressions of constitutive equations of the poroelastic medium are given as in [2]:

$$\underline{\underline{\sigma}} - \underline{\underline{\sigma}}_0 = \underline{\underline{C}} : \underline{\underline{\varepsilon}} - \underline{\underline{b}}(p - p_0) \quad (1)$$

$$\phi - \phi_0 = \underline{\underline{b}} : \underline{\underline{\varepsilon}} + \frac{(p - p_0)}{M} \quad (2)$$

The local momentum and fluid mass balance equations in the context of infinitesimal skeleton strains are shown in Eq. (3) and Eq. (4) respectively:

$$\text{div} \underline{\underline{\sigma}} + \rho \underline{\underline{g}} = 0 \quad (3)$$

$$\rho \frac{\partial \phi}{\partial t} + \text{div}(\underline{\underline{q}}_f) = 0 \quad (4)$$

Where a Darcy law in limit quasi-static is:

$$\underline{\underline{q}}_f = \underline{\underline{k}} \cdot (-\nabla p + \rho^f \underline{\underline{g}}) \quad (5)$$

Where  $\underline{\underline{\sigma}}$  is the stress tensor,  $\underline{\underline{C}}$  is the drained stiffness tensor,  $\underline{\underline{\varepsilon}}$  is the strain tensor,  $\underline{\underline{b}}$  is the Biot effective stress coefficient tensor,  $p$  is the pore pressure,  $\underline{\underline{g}}$  is the acceleration of gravity,  $\rho$  is the density of the porous material ( $\rho = \phi \rho^f + (1 - \phi) \rho^s$ ), which can be computed from the Eulerian porosity  $\phi$  (i.e. the pore volume fraction in the current configuration), the fluid density  $\rho^f$  and the solid grains density  $\rho^s$ ,  $\phi$  is the Lagrangian porosity,  $M$  is the Biot modulus,  $\underline{\underline{q}}_f$  is the filtration vector,  $\underline{\underline{k}}$  is the permeability tensor.

### 1.2 Analytical and semi-analytical solutions

In the literature was presented an analytical solution for deep tunnels in Coussy [2] for times shorter than the characteristic time of hydraulic diffusion ( $t \ll \tau$ ) and plane deformation, this solution is shown in Eq. (7) and Eq. (8).

$$\tau = \frac{R_i^2}{c^f} \quad (6)$$

$$p(r, t) = p_\infty + (p_i - p_\infty) \bar{p}(r, t). \quad (7)$$

$$\bar{p}(r, t) = \sqrt{\frac{R_i}{r}} \left[ 1 - \text{erf} \left( \frac{r - R_i}{2\sqrt{c^f t}} \right) \right] - \frac{1}{8} \sqrt{\frac{R_i}{r}} \frac{r - R_i}{2r} \left[ \frac{2}{\sqrt{\pi}} \frac{\sqrt{c^f t}}{R_i} \exp \left( -\frac{(r - R_i)^2}{4c^f t} \right) - \frac{r - R_i}{R_i} \left( 1 - \text{erf} \left( \frac{r - R_i}{2\sqrt{c^f t}} \right) \right) \right] \quad (8)$$

Where  $p(r, t)$  is the poropressure at a distance  $r$  and a time  $t$ ,  $p_\infty$  is the initial poropressure,  $p_i$  is

the poropressure at the tunnel wall,  $R_i$  is the internal radius of the tunnel,  $c^f$  is the fluid diffusivity coefficient.

For any time in general form is presented a semi-analytical solution shown in Carslaw e Jaeger [3]. The solution is supported with the Stehfest algorithm and is shown in Eq. (9), Eq. (10), Eq. (11), and Eq. (12).

$$p(r,t) = p_\infty + \delta p(r,t). \quad (9)$$

$$\delta p(r,t) = \frac{\ln(2)}{t} \sum_{n=1}^N c_n \overline{\delta p} \left( r, n \frac{\ln(2)}{t} \right). \quad (10)$$

$$c_n = (-1)^{n+\frac{N}{2}} \sum_{k=E(\frac{n+1}{2})}^{Min(n,N/2)} \frac{k^{N/2} (2k)!}{(N/2-k)! k! (k-1)! (n-k)! (2k-n)!}. \quad (11)$$

$$\overline{\delta p}(r,s) = \frac{p_i - p_\infty}{s} \frac{K_0(qr)}{K_0(qR_i)}. \quad (12)$$

Where  $p(r,t)$  is the poropressure at a distance  $r$  at a time  $t$ ,  $p_\infty$  is the initial poropressure,  $\overline{\delta p}(r,s)$  is the Laplace transform,  $k!$  is the factorial of a natural number,  $E(x)$  designates the whole number of  $x$ ,  $Min(a,b)$  designates the minimum of  $a$  and  $b$ ,  $K_0$  is the modified Bessel of second kind and order 0,  $N$  is a natural number greater than or equal to 6.

## 2 Finite Element Implementation

Making the temporal and spatial discretization of the Eq. (1), Eq. (2), Eq. (3), Eq. (4) and Eq. (5) and following the approach of Sandhu and Wilson [4], we get the array shown in (13):

$$\begin{bmatrix} \underline{\underline{K}}_{UU} & \underline{\underline{K}}_{UP} \\ \underline{\underline{K}}_{PU} & \underline{\underline{K}}_{PP} \end{bmatrix} \begin{bmatrix} \underline{U} \\ \underline{P} \end{bmatrix} = \begin{bmatrix} \underline{F}_U \\ \underline{F}_P \end{bmatrix}. \quad (13)$$

The first line of the system corresponds to the momentum balance equation, and the second line corresponds to the fluid mass balance equation. The sub-matrix  $\underline{\underline{K}}_{UU}$  represents the terms of internal stress. The sub-matrices  $\underline{\underline{K}}_{UP}$  and  $\underline{\underline{K}}_{PU}$  are symmetric and correspond to the terms of hydro-mechanical coupling. The sub-matrix  $\underline{\underline{K}}_{PP}$  represents the pressure terms.  $\underline{F}_U$  and  $\underline{F}_P$  are the vectors of force and pressure,  $\underline{U}$  e  $\underline{P}$  represents the variation of displacements and pressures respectively.

As performed by Bruch [5], the finite element used in numerical modeling is based on the element superposition method. For the approximation of the displacements, a quadratic isoparametric element of 20 nodes is used, with three degrees of freedom per node. To approximate the pore pressure, the 8-node linear hexahedral element is used, with one degree of freedom per node, therefore is obtained:

$$\underline{\underline{K}}_{UU} = \int_{V_e}^T \underline{B}_{es} \cdot {}^t C_{es} \cdot \underline{B}_{es} dV_e. \quad (14)$$

$$\underline{\underline{K}}_{UP} = {}^T \underline{\underline{K}}_{PU} = - \int_{V_e} {}^t b^T \underline{B}_{es} \cdot \underline{1} \cdot \tilde{N}_e dV_e. \quad (15)$$

$$\underline{\underline{K}}_{PP} = -\int_{V_e} \frac{1}{M} {}^T \tilde{N}_e \cdot \tilde{N}_e dV_e - \delta t \int_{V_e} {}^t k {}^T \tilde{\underline{\underline{B}}}_e \cdot \tilde{\underline{\underline{B}}}_e dV_e. \quad (16)$$

$$\underline{F}_U = -\int_{V_e} {}^T \underline{\underline{B}}_{es} \cdot {}^t \underline{\underline{\sigma}}_e dV_e + \int_{S_e^T} {}^T \underline{N}_e \cdot {}^t \underline{T}_e^d dS_e^T + \int_{V_e} {}^t \rho {}^T \underline{N}_e \cdot \underline{g}_e dV_e. \quad (17)$$

$$\underline{F}_p = +\delta t \int_{V_e} {}^t k {}^T \tilde{\underline{\underline{B}}}_e \cdot \tilde{\underline{\underline{B}}}_e \cdot {}^t \underline{p}_e dV_e - \delta t \int_{V_e} {}^t k \rho^f {}^T \tilde{\underline{\underline{B}}}_e \cdot \underline{g}_e dV_e + \delta t \int_{S_e^Q} {}^t q_e^d {}^T \tilde{N}_e dS_e^Q. \quad (18)$$

The arrays and vectors used are shown below:

$$\underline{\underline{N}}_{e(3 \times 60)} = \begin{bmatrix} N_1 & 0 & 0 & & N_{20} & 0 & 0 \\ 0 & N_1 & 0 & \dots & 0 & N_{20} & 0 \\ 0 & 0 & N_1 & & 0 & 0 & N_{20} \end{bmatrix}. \quad (19)$$

$$\tilde{\underline{N}}_{e(1 \times 8)} = [\tilde{N}_1 \quad \dots \quad \tilde{N}_{20}]. \quad (20)$$

$$\tilde{\underline{\underline{B}}}_{e(3 \times 8)} = \begin{bmatrix} \frac{\partial \tilde{N}_1}{\partial x} & & \frac{\partial \tilde{N}_8}{\partial x} \\ \frac{\partial \tilde{N}_1}{\partial y} & \dots & \frac{\partial \tilde{N}_8}{\partial y} \\ \frac{\partial \tilde{N}_1}{\partial z} & & \frac{\partial \tilde{N}_8}{\partial z} \end{bmatrix}. \quad (21)$$

$$\underline{\underline{B}}_{es(6 \times 60)} = \begin{bmatrix} \frac{\partial N_1}{\partial x} & 0 & 0 & & \frac{\partial N_{20}}{\partial x} & 0 & 0 \\ 0 & \frac{\partial N_1}{\partial y} & 0 & \dots & 0 & \frac{\partial N_{20}}{\partial y} & 0 \\ 0 & 0 & \frac{\partial N_1}{\partial z} & & 0 & 0 & \frac{\partial N_{20}}{\partial z} \\ \frac{1}{2} \frac{\partial N_1}{\partial y} & \frac{1}{2} \frac{\partial N_1}{\partial x} & 0 & & \frac{1}{2} \frac{\partial N_{20}}{\partial y} & \frac{1}{2} \frac{\partial N_{20}}{\partial x} & 0 \\ 0 & \frac{1}{2} \frac{\partial N_1}{\partial z} & \frac{1}{2} \frac{\partial N_1}{\partial y} & \dots & 0 & \frac{1}{2} \frac{\partial N_{20}}{\partial z} & \frac{1}{2} \frac{\partial N_{20}}{\partial y} \\ \frac{1}{2} \frac{\partial N_1}{\partial z} & 0 & \frac{1}{2} \frac{\partial N_1}{\partial x} & & \frac{1}{2} \frac{\partial N_{20}}{\partial z} & 0 & \frac{1}{2} \frac{\partial N_{20}}{\partial x} \end{bmatrix}. \quad (22)$$

$${}^T \underline{\underline{\sigma}}_{e(6 \times 1)} = [\sigma_{xx} \quad \sigma_{yy} \quad \sigma_{zz} \quad \sigma_{xy} \quad \sigma_{yz} \quad \sigma_{xz}]. \quad (23)$$

$${}^T \underline{P} = {}^T \underline{P}_{e(8 \times 1)} = [P_1 \quad \dots \quad P_8]. \quad (24)$$

$${}^T \underline{T}_{e(3 \times 1)} = [T_x \quad T_y \quad T_z]. \quad (25)$$

Where the matrix  $N_i$  is the shape functions,  $\underline{\underline{C}}_e$  is the elasticity matrix containing the material properties,  ${}^t b$  is the coefficient of Biot,  ${}^t M$  is the Biot Modulus,  $\underline{g}_e$  is the vector of acceleration of gravity,  ${}^t \rho$  is the density of the porous material,  ${}^t k$  is the coefficient of permeability and  $\delta t$  is the time interval.

### 3 Implementation of the excavation process

#### 3.1 Excavation process in a poroelastic medium

For deactivate an element (element excavated), physical parameters of the material are changed to obtain stresses and pore-pressures that tends to zero.

From equation (2), the pore-pressures variation  $\Delta p$  can be written as:

$$\Delta p = M \left( \Delta \phi - \underline{b} : \underline{\underline{\varepsilon}} \right). \quad (26)$$

The condition of  $\Delta p = 0$  (in the excavated elements), is obtained when  $M \approx 0$ , i.e.  $M_{esc} \ll M$  (The value of the Biot module of the excavated elements  $M_{esc}$  is considerably smaller than the Biot modulus of the rest of the rockmass  $M$  ).

From equation (1), the vector of tensions can be written as:

$$\Delta \underline{\underline{\sigma}} = \underline{\underline{C}} : \underline{\underline{\varepsilon}} - \underline{\underline{b}} \Delta p. \quad (27)$$

In the excavated elements, the vector  $\Delta \underline{\underline{\sigma}}$  is zero when  $\underline{\underline{C}} \approx 0$ , since  $\Delta p$  is null (due the previous condition), in consequence  $E \approx 0$ , i.e.  $E_{esc} \ll E$  (The Young's modulus of the excavated elements  $E_{esc}$  is considerably smaller than the Young's modulus of the rest of the rockmass  $E$  ).

The flow vector can be written as:

$$\underline{\underline{q}}_f = \underline{\underline{k}} \cdot (-\nabla p + \rho^f \underline{\underline{g}}). \quad (28)$$

Since the value  $\nabla p = 0$ , the permeability tensor  $\underline{\underline{k}}$  must tend to infinity.

## 4 Applications

#### 4.1 Bi-dimensional analysis of a deep tunnel

An analysis considering the case of plane strain deformation, showing the analytical, semi-analytical and numerical solution is presented. The numerical solution is implemented with finite element method and is based within the framework of the quasi-static Biot's theory of poroelasticity [6].

It is considered an unlined circular tunnel of radius  $R = 1 \text{ m}$ , through an poro-elastic and saturated medium subjected to total isotropic in situ stress  $\sigma_{xx} = \sigma_{zz} = 4 \text{ Mpa}$  and initial hydrostatic pore pressure of  $p_0 = 2 \text{ Mpa}$ . The ground properties are given in Table 1, while the layout of the tunnel model and the corresponding boundary conditions are shown in Fig. 2. Is modeled the fourth part of the model taking advantage of the symmetry, the model boundaries are impermeable, except those at the tunnel wall, where the pressure pore is equal to zero.

Table 1. Ground properties

$E =$	200 Mpa	Young's modulus
$\nu =$	0.25	Poisson's ratio
$k =$	$4 \cdot 10^{-12} \text{ m/s}$	Hydraulic conductivity
$M =$	7500 Mpa	Biot's modulus
$b =$	1	Biot's coefficient
$\rho =$	$1200 \text{ kg/m}^3$	Rock specific weight
$\gamma_w =$	$9807 \text{ N/m}^3$	Fluid volumetric weight
$g =$	$9.80665 \text{ m/s}^2$	Gravitational acceleration

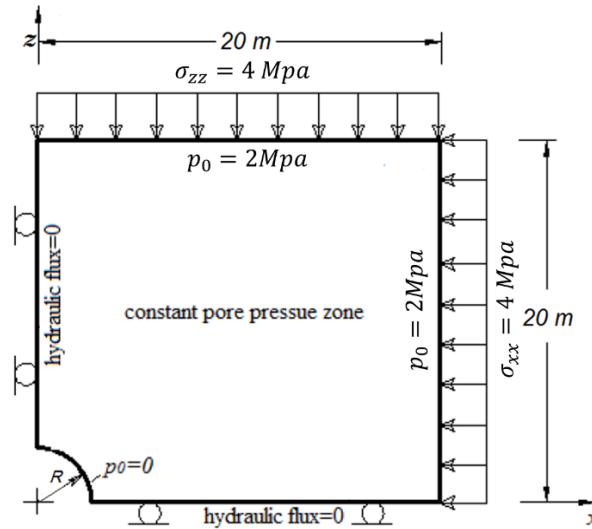


Figure 2. Illustrations of model layout and boundary conditions

The characteristic time is calculated with the Eq. (22):

$$\tau = \frac{R_i^2}{\left(\frac{k}{\gamma_w g}\right)} \cdot \left(\frac{1}{M} + \frac{b^2(1+\nu)(1-2\nu)}{E(1-\nu)}\right) = 122 \text{ days} \quad (29)$$

The analytical solution shown in Coussy [2] was corroborated, confirming that this solution is valid for times shorter than the characteristic time ( $\tau$ ). In this interval the analytical solution coincides with the semi-analytical solution shown in Carslaw and Jaeger [3] (Fig. 3).

The semi-analytical solution is valid for any time and matches with the numerical solution. The numerical solution is evaluated in two ways: The first considers the existing tunnel and the second consider the intact rockmass and then applying the excavation process (in a single step). Both numerical solutions are similar, thus validating the excavation process (Fig. 3).

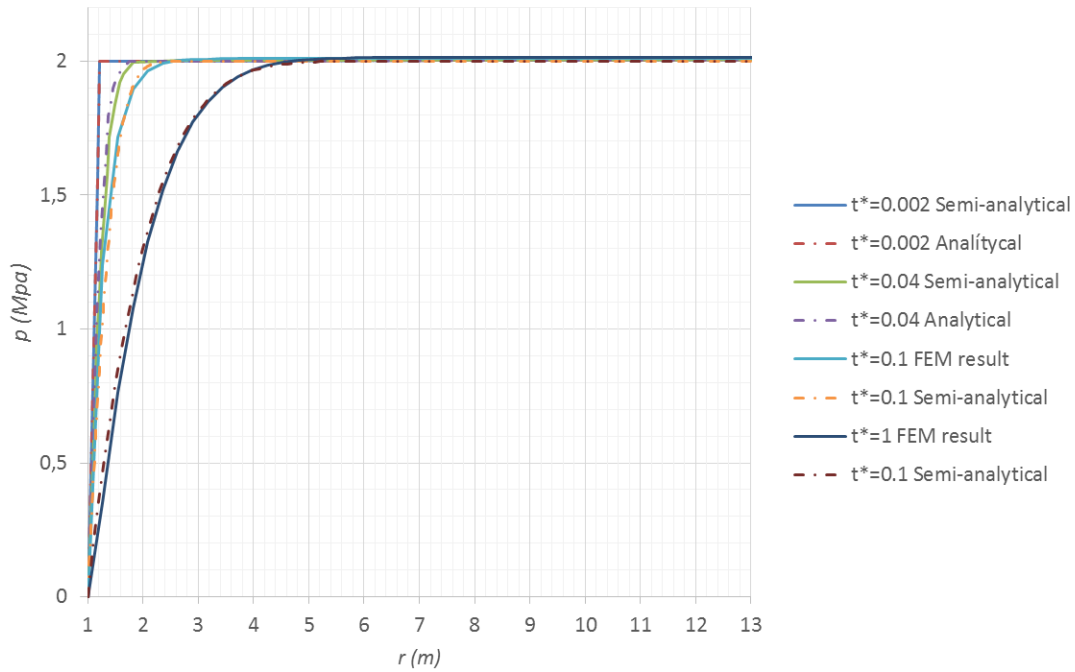


Figure 3. Pore pressure versus o radius

#### 4.2 Tri-dimensional analysis of a deep tunnel

The analysis presented consider the tridimensional case. The numerical solution is implemented with finite element method and is based within the framework of the quasi-static Biot's theory of poroelasticity [6], the results are compared with the results obtained by Prassetyo and Gutierrez [7].

It is considered an unlined circular tunnel of radius  $R = 2.5 \text{ m}$ , through an poro-elastic and saturated medium subjected to total isotropic in situ stress  $\sigma_{xx} = \sigma_{zz} = 4.5 \text{ Mpa}$  and initial hydrostatic pore pressure of  $p_0 = 2.25 \text{ Mpa}$ . The ground properties are given in table 2, while the layout of the tunnel model and the corresponding boundary conditions are shown in Fig. 4. It is modeled the fourth part of the model taking advantage of the symmetry, the model boundaries are impermeable, except those at the tunnel wall, where the pressure pore is equal to zero.

Table 2. Ground properties

$E =$	$292.5 \text{ Mpa}$	Young's modulus
$\nu =$	$0.125$	Poisson's ratio
$k =$	$5 \cdot 10^{-10} \text{ m/s}$	Hydraulic conductivity
$M =$	$5096 \text{ Mpa}$	Biot's modulus
$b =$	$1$	Biot's coefficient
$\rho =$	$1200 \text{ kg/m}^3$	Rock specific weight
$\gamma_h =$	$9807 \text{ N/m}^3$	Fluid volumetric weight

An excavation process is simulated by progressively deactivating 40 regions of width  $\Delta y = 1.25 \text{ m}$ , from  $y = 0$  to  $y = 50 \text{ m}$ , implying an excavation rate of  $5 \text{ m/day}$ . During the excavation process, the face is instantaneously removed for a period of  $\Delta t = 0$  (undrained loading), followed by drained consolidation for a period of  $\Delta t = 1/4 \text{ day}$  (drained loading) at each excavation step.

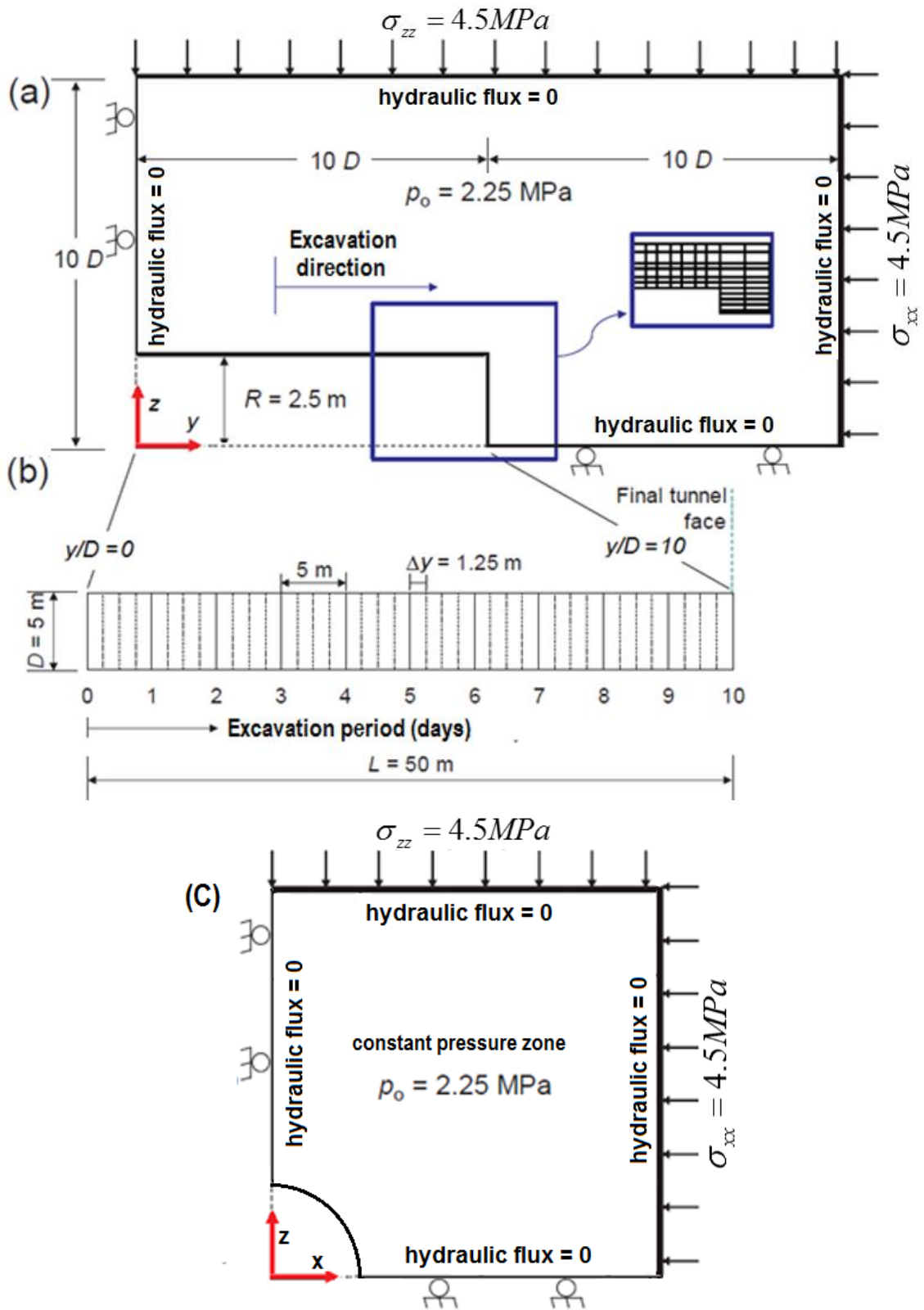


Figure 4. Illustrations of model layout with (a) longitudinal boundary conditions (b) excavations steps (c) transversal boundary conditions adapted from Gutierrez and Prassetyo [7]

The Figure 5 shows a displacement in the wall of the tunnel (convergence), at  $y=25\text{ m}$ , during the excavation period. This displacement starts to drop at  $t=3\text{ days}$ , and quickly increases to  $-3\text{ cm}$  at  $t=5\text{ days}$  then keep increasing as the face advances até  $t=10\text{ days}$  when the displacement results in  $-4.24\text{ cm}$ . Also is shown an axisymmetric analysis of Prassetyo and Gutierrez [7] that have similar values.

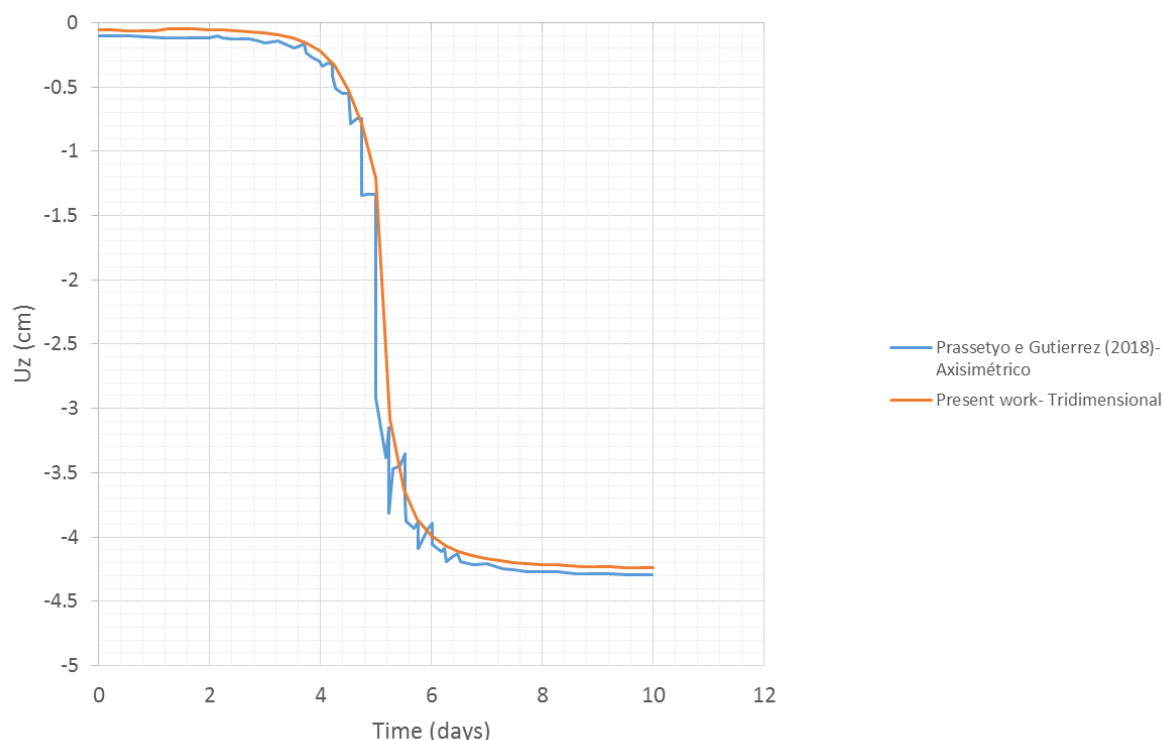


Figure 5. Transient hydraulic-mechanic response of the convergence during the excavation period using the progressive step by step excavation

The Figure 6 shows a displacement in the wall of the tunnel (convergence) along the tunnel axis, when a face is at  $y=25\text{ m}$ , allowing a consolidation during  $t=920\text{ days}$  after the excavation. This results shows the expected behavior of the displacement, comparing with the results of Prassetyo and Gutierrez [7]. similar values of convergence are observed at the face of the tunnel.

The Figure 7 shows a pore pressure at 1m above the wall of the tunnel at  $y=25\text{ m}$ , during the excavation period. The pore pressure starts to increase slowly to reache the peak value of  $2.33\text{ MPa}$  at  $t=4.5\text{ days}$  and drops to  $1.56\text{ MPa}$  at the monitoring point at  $t=5\text{ days}$ . The pore pressure continues to fall as the tunnel face passes the monitoring point and it starts to decrease more steadily at  $t=5.25\text{ days}$ , after continue decreasing with similar slope. Comparing with the results of Prassetyo and Gutierrez [7], similar value of pore pressure is observed at the face of the tunnel ( $y=25\text{ m}$ ), the differences must be due to the type of analysis, mesh difference of the finite elements and considerations of drained/undrained conditions.

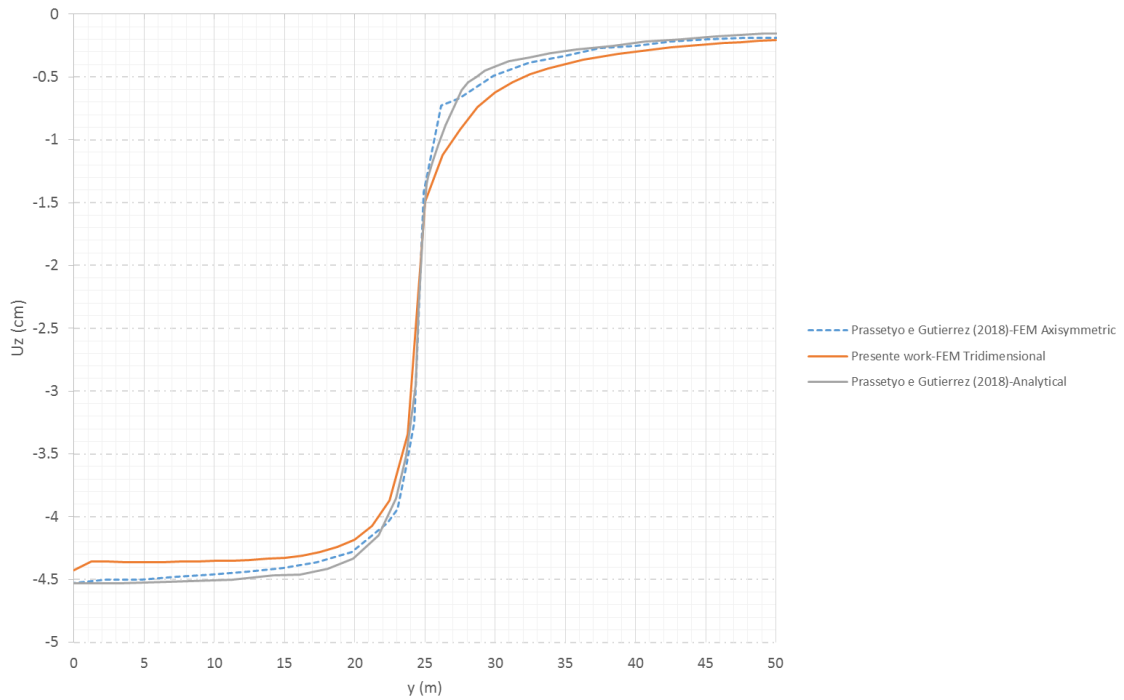


Figure 6. Plots of radial displacements after finish the excavation when  $t = 920$  days

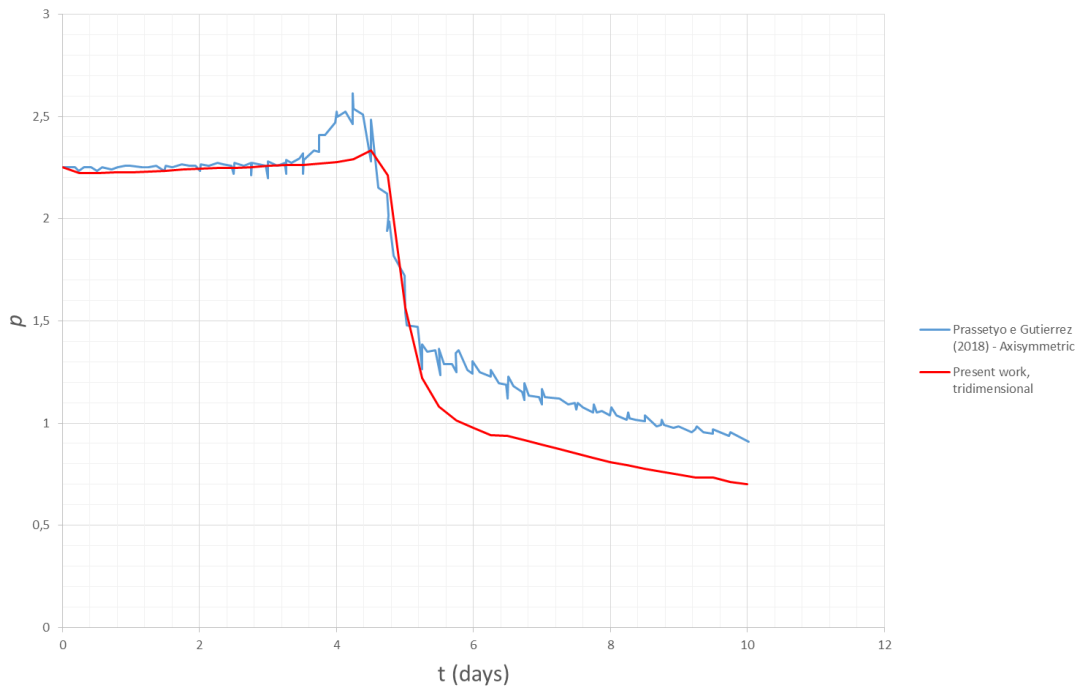


Figure 7. Transient hydraulic-mechanic response of the porepressure during the excavation period using the progressive step by step excavation

## 5 Conclusions

A simulation is carried out for the excavation process in a poroelastic medium, that was modeled using the Biot theory and the excavation using the activation/deactivation method. For the deactivation of the elements it is considered a very small values of Young Modulus and Biot Modulus and very large values of permeability. With these considerations we obtained similar values of the analytical, semi-analytical and numerical solutions for the case of plane strain deformation.

When the excavation takes place (in a saturated mass), the initial tensions in the rockmass change due to the excavation and the forces of infiltration. The infiltration flow follows the direction from which the material is removed because the pressure at the excavation boundary is generally atmospheric and the mass around the tunnel acts such a draining wall. Due to this effect in vicinity of the tunnel, the convergence increases compared to the unsaturated case, while the face of the tunnel advances the convergence increases until reaching the maximum convergence.

## Acknowledgements

Gratefully acknowledge the important support of CNPq (in Portuguese “Conselho Nacional de Desenvolvimento Científico e Tecnológico”).

## References

- [1] C. Carranza-Torres and C. Fairhurst. Application of the convergence-confinement method of tunnel design to rock masses that satisfy the Hoek-Brown failure criterion. *Tunnelling and Underground Space Technology* vol. 15, n. 2, pp. 187-199, 2000.
- [2] O. Coussy. *Poromechanics*. John Wiley & Sons, 2004.
- [3] H. Carslaw and J. Jaeger. *Conduction of heat in solids*. Oxford Clarendon Press, 1959.
- [4] R. Sandhu and E. Wilson. Finite-element analysis of seepage in elastic media. *Journal of the Engineering Mechanics Division*, vol. 95, n. 3, pp. 641-652, 1969.
- [5] A. Bruch. Simulação numérica tridimensional de processos de deformação em bacias sedimentares. PhD thesis, Universidade Federal do Rio Grande do Sul, 2016.
- [6] M. Biot. General theory of three-dimensional consolidation. *Journal of applied physics*, vol. 12, n. 2, pp. 155-164, 1941.
- [7] S. Prassetyo and H. Gutierrez. Effect of transient coupled hydro-mechanical response on the longitudinal displacement profile of deep tunnels in saturated ground. *Tunnelling and Underground Space Technology*, vol. 75, n. 1, pp. 11-20, 2018.